Environ Geol
DOI 10.1007/s00254-008-1642-0

ORIGINAL ARTICLE

The identified origin of a linear slope near Chi–Chi earthquake rupture combining 2D, 3D resistivity image profiling and geological data

Cheng-Chao Lee · Louis Loung-Yie Tsai · Chieh-Hou Yang · Kuo-Liang Wen · Zi-Bin Wang · Zhi-Hsian Hsieh · Hsing-Chang Liu

Received: 12 September 2008 / Accepted: 28 October 2008

Abstract A slope on the west border of the foothill near 921 surface rupture (caused by the 1999 Chi-Chi earthquake) in central Taiwan shows distinctive topographic expression that was prone to be considered as a fault scarp formed by a preexisting active fault. The 2D and 3D resistivity images clearly delineate rock surfaces which show steep, deep, gentle, and subvertical displacement beneath the slope, the toe of slope, the non-lateritic terrace, and 921 surface rupture, respectively, which can be attributed to the significant contrast of resistivity between gravel and rock. The horizontal sand bed and clast-supported gravel were deposited in a fluvial environment, whereas wedge-shaped gravel and colluvium were scarp-induced colluvial deposits in the trench profile. The layers shown in the depth of excavation, except for rock, has no offset or disturbance by fault ever since at least 2,480 ± 50 year B.P., based on carbon 14 dating of charcoal sample at the bottom of trench profile. According to information from two boreholes close to the slope, an over 20-m-thick marker bed with transported shell fragments, was found for correlation. This correlation further implies the slope was not formed by fault. On the other hand, two boreholes which are far from the slope and located on the flat non-lateritic terrace frequently show fractured and sheared features. By comparison, the locations around these two boreholes indicate a reverse fault or faults that occurred before the deposition of gravel. Later on, the paleostream was developed along the foot of fault scarp that was subjected to erosion and led to subsequent retrogression or retreat of the slope. Consequently, the incision of paleostream is believed to be responsible for the high relief of rock surface around the slope. Furthermore, from resistivity and borehole data, the rock surface underlying terrace is gentle where no faults occur after the deposition of gravel. The result of RIP crossing the 921 surface rupture displays about 10 m difference in elevation of rock surface on both sides, which is greater than that of 3–4 m caused by Chi-Chi earthquake. This indicates that the 921 surface rupture is a preexisting thrust fault that resulted from several thrusting events since terrace gravel was deposited. So it is not necessary to establish an extra restricted zone for construction in study area, except close to the 921 surface rupture.

Keywords 921 surface rupture · Chelungpu fault · Resistivity · Zone for construction · Gravel

C.-C. Lee (✉) · K.-L. Wen · Z.-H. Hsieh · H.-C. Liu
Institute of Geophysics, National Central University,
No. 300, Jhongda Road, Jhongli City,
Taoyuan County 320, Taiwan, ROC
e-mail: lcc@sinogeotech.com.tw

L. L.-Y. Tsai
Institute of Applied Geology, National Central University,
No. 300, Jhongda Road, Jhongli City,
Taoyuan County 320, Taiwan, ROC

C.-H. Yang · Z.-B. Wang
Department of Engineering, Ching-Yun University,
No. 229, Chien-Hsin Road, Jhongli City,
Taoyuan County 320, Taiwan, ROC

Introduction

921 surface rupture, induced by the September 21, 1999 Chi-Chi earthquake ($M_L = 7.3$) which was caused by reactivation of the Chelungpu Fault, generated great displacement and surface deformation in central Taiwan. The Chelungpu Fault is defined as the Pliocene Formation thrust onto the modern terrace sediments, which is located along the boundary between the Western Foothills and Taichung piggyback basin with distinctive topographic

feature (Ho 1959, 1976; Meng 1963; Pan 1967; Chang 1971; Bonilla 1977; Hsu and Chang 1979; Chang et al. 1998) (Fig. 1). Although the northern part of 921 surface rupture approximately follows the border of the Western Foothills, it occurs in the hanging wall of the Chelungpu fault, where no active fault or any positive evidence such as terrace or overburden being penetrated by fault had been previously reported. The local and small ruptures were also found in the east side of the 921 surface rupture during the Chi-Chi earthquake (CGS 1999; Chen et al. 2003). In addition, several terraces with different elevation were found in the hanging wall, which suggests the high slip rate of uplift caused by a reverse fault (Chen et al. 2000, 2003; Tsai and Sung 2003; Lai et al. 2006). The surface deformation of Chi-Chi earthquake near Fengyuan is believed to be closely related to the imbricate splay faults at a shallow depth, which are usually associated with a thrust fault zone on the surface (Huang et al. 2000). 921 surface rupture that occurred during the Chi-Chi earthquake may be one of the branch faults. Therefore, any slope with topographic expression near the 921 surface rupture was suspected to be probably caused by preexisting reverse fault.

The orientation of 921 surface rupture shows two directions near Fengyuan, from N to S in the south of

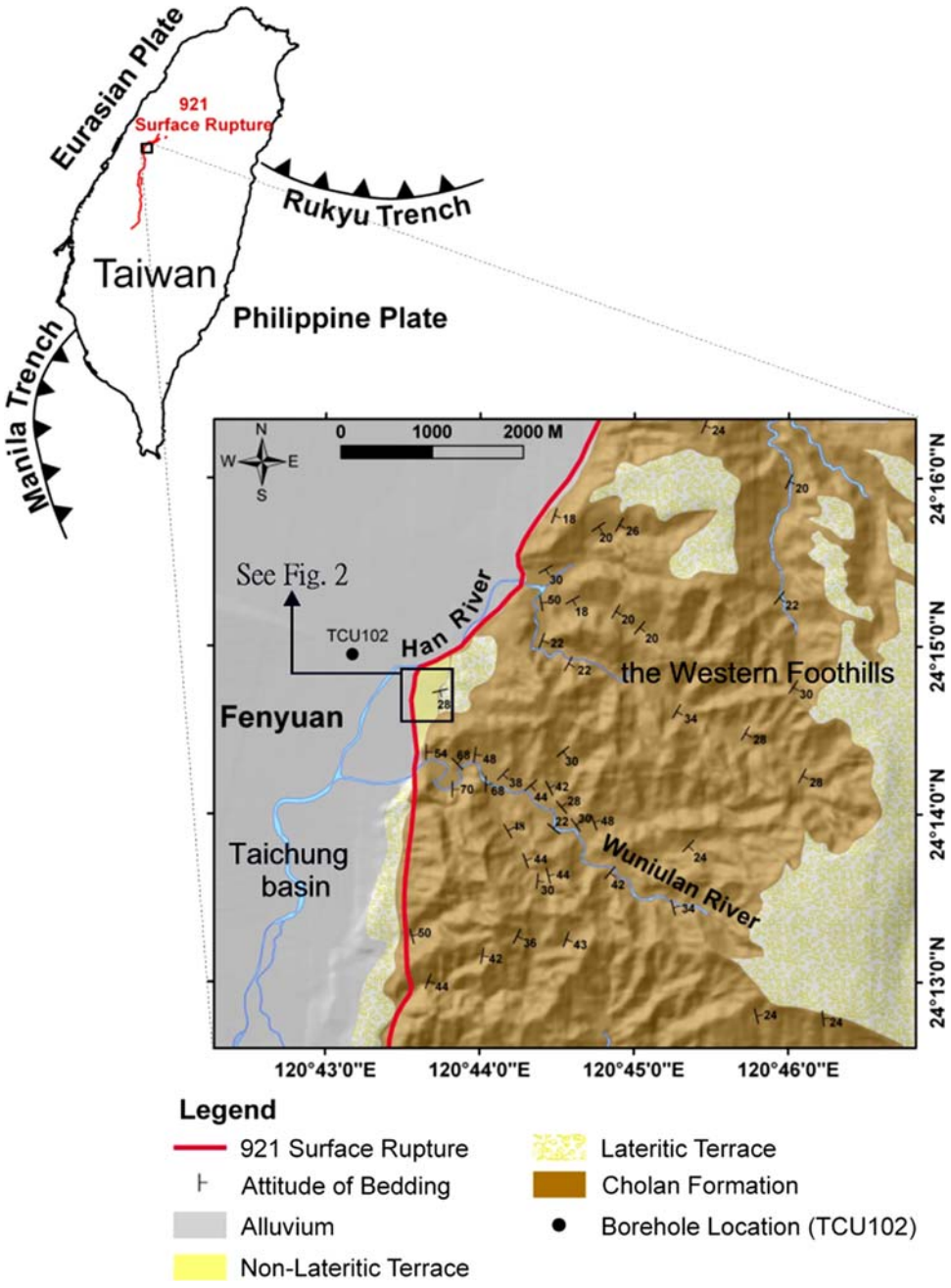

Fig. 1 Geological map of the study area and its surroundings. The trend of 921 surface rupture was changed from N–S in the south of Wuniulan river to NE–SW in the north of Han river

Wuniulan River to NE–SW in the north of Han River (Fig. 1). It is odd that the surface rupture between Wuniulan River and Han River departed from the border of the Western Foothills and followed the western border of non-lateritic terrace. The distinctive N20°E trending topographic feature, located east of the 921 surface rupture, is a 15-m high and west-facing slope (Fig. 2). This slope was considered as a fault scarp caused by preexisting active fault (Ota et al. 2003, 2004, 2007). The existence and exact location of the active fault is critical for evaluating earthquake risk and their identification is therefore needed.

According to geological characteristics in this area, lithologic distribution, especially in the geometry of gravel and contact surface between gravel and rock, is important for understanding the origin and evolution of this slope. Combing 2-D and 3-D resistivity image profiling (RIP) technique is used as efficient tools to investigate the shallow depth such as a few to tens of meters. Many successful cases to detect active fault in this depth were published (Suzuki et al. 2000; Nguyen et al. 2007; Vanneste et al. 2008). Previous geoelectrical studies focused on the the northern tip and the middle to southern part of the Chelungpu fault also gained good results (Cheng 2000; Cheng et al. 2002; Yang

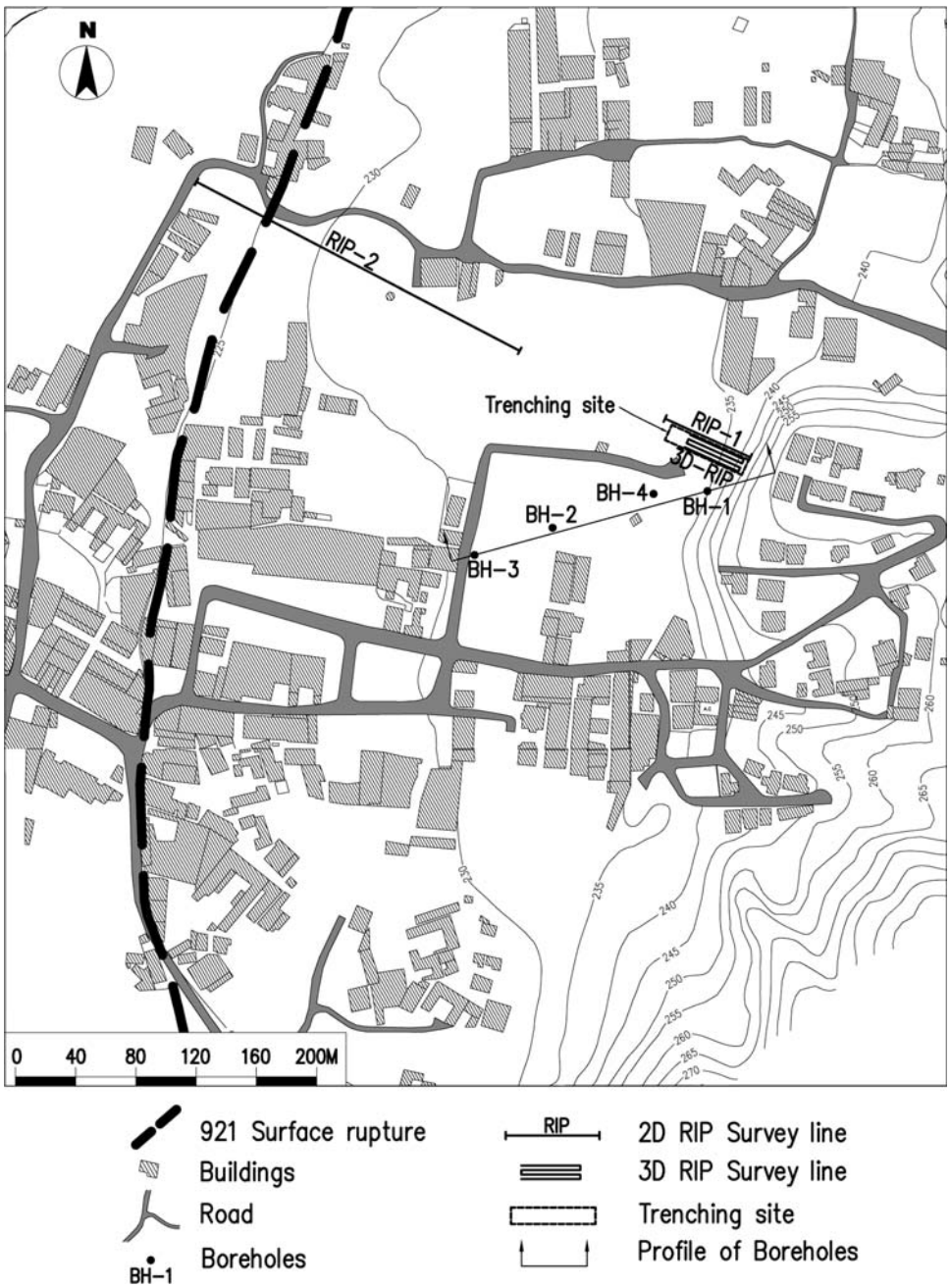

Fig. 2 Survey area map. A 15 m high, west-facing slope with N20°E trending can be observed

et al. 2002). The advantage of RIP survey is that higher resolution can be obtained than that of other methods such as seismic reflection due to high contrast in resistivity between gravel and rock in this site. Furthermore, trench excavation in the toe of slope and borehole sampling was carried out, which can directly verify the results of geoelectrical survey and provide more detailed characteristics of rock for geological interpretation and evolution of the study area.

Geological setting

Taiwan is located along the oblique collision zone between the Philippine Sea plate and Eurasian plate (Fig. 1). The study area is located on the west-central part of Taiwan. There are three distinct geological provinces: the Western Foothills in the east, Taichung basin in the west, and river terrace in between. The Plio-Pleistocene Cholan Formation in the foothill is composed of 1,500–2,500 m of sandstone, siltstone, mudstone, and shale in a monotonous alternating sequence. Facies changes are rapid in this thick clastic sequence, and no key beds have been found to subdivide this formation into distinct members (Lee 2000). River terrace consists mainly of gravel which uncomformably overlies the Cholan Formation, the lower and non-lateritic terrace is distributed between east of the Cholan Formation and west of a flat alluvium, the higher and lateritic terrace is located on the western margin of the Western Foothills. The widespread alluvium, which is composed of gravel, sand, and clay, covers the Taichung basin.

The Plio-Pleistocene Cholan Formation in the foothill shows the monoclinic structure and dips to the east at angles from 25 to 45 degrees (Ho and Chen 2000). The Chelungpu fault is one of the major geological structures which runs approximately along the eastern margin of the Taichung basin and extends north-southwards (Ho and Chen 2000) (Fig. 1). The western border of non-lateritic terrace surface with minor west-dip, west of the Western Foothills and between Wuniulan River and Han River, was obscure and not easily identifiable before Chi-Chi earthquake. However, it was clear after the uplifting of 3–4 m by Chi-Chi earthquake, even though the lithology of basement were same on its both sides. It differs from the middle to southern part of the Chelungpu fault where the Pliocene formation was located on the hanging wall and gravel on the foot wall.

Resistivity image profiling (RIP) method

2D RIP

Resistivity image profiling (RIP) is an active prospecting method used for yielding a high-resolution image of subsurface patterns of electrical resistivity. High-definition pseudosections were quickly acquired by dense sampling of apparent resistivity variation at shallow depths. Resistivity data were acquired by using McOHM2115 manufactured by OYO, Japan with pole-pole array (Fig. 3), which has the widest horizontal coverage and the deepest depth of investigation (Loke 2001). The significant difference between pole-pole array and other arrays is that a current electrode and a potential electrode (served as remote electrodes) were positioned at a distance of 10 times the expected depth of exploration from the survey line. Theoretically, the depth of the investigation is proportional to the length of profile. The shorter the electrode spacing, especially at shallow depth, the higher the data density and resolution will be. To obtain true resistivity distribution of surface, the authors used RES2DINV for inversion. This resistivity software was based on 2.5D smoothness-constrained inversion, employing a quasi-Newton technique to reduce numerical calculations (Loke and Barker 1996). The final geoelectrical models show a root mean square (rms) error of 5.2–8.9% after five iterations. For the purpose of smoothing the variation of iso-resistivity color bands, the final profiles were displayed by Surfer software.

3D RIP

With the development of multi-channel equipment and inversion techniques, 3D RIP is becoming more common and is used to detect more detailed subsurface resistivity

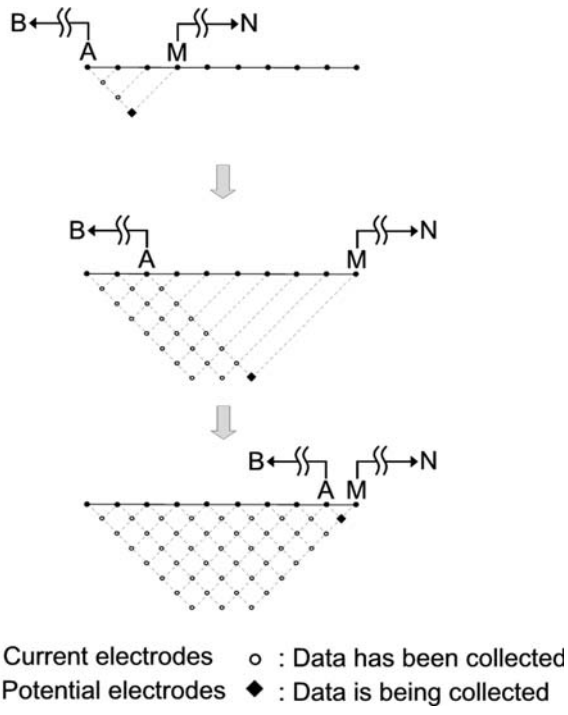

Fig. 3 RIP survey using a pole–pole array

variation, which gives the most accurate result (Loke 2001). The 3D RIP of this study was conducted using a system of 56 electrodes, which covered a rectangular area and were arranged in a 4 × 14 grid with a pole-pole array that measures the complete data set in all possible directions of every electrode (Fig. 4). Resistivity data obtained in the field by Sting R1/IP manufactured by AGI, USA was inverted to true resistivity structure by using RES3DINV, which is based on the smoothness-constrained least-squares method using the quasi-Newton optimization technique (Loke and Barker 1996). The final geoelectrical model shows a root mean square (rms) error of 6.52% after six iterations. For the purpose of smoothing the variation of iso-resistivity color bands, the final three-dimensional images were displayed by Voxler software.

RIP results

The relation between resistivity and lithological character in the study area and related study of the Chelungpu Fault (Cheng 2000; Cheng et al. 2002; Yang et al. 2002), reveal that the resistivity of the gravel is higher than 120 Ω-m at least, and the resistivity of sandstone is higher than that of muddy sandstone and shale (which is less than 60 Ω-m). In addition, the resistivity of sand bed is between 50 and 200 Ω-m, depending on its moisture content.

The RIP-1 was deployed perpendicular to the orientation of the slope (Fig. 2). 1 m of electrode spacing was chosen for the higher resolution at shallow depth, but with limited depth of investigation. As shown in Fig. 5(a), a subvertical interface between the position 42 and 47 m has distinctive

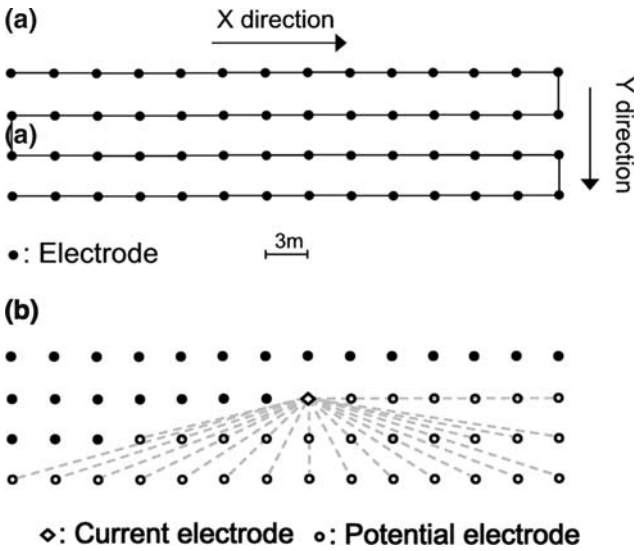

Fig. 4 **a** The arrangement of 3D RIP survey. X and Y directions are perpendicular and parallel to the slope, respectively. **b** The complete data set measured for 3D RIP survey

contrast in resistivity on both sides. The resistivity zone less than 50 Ω-m on the eastern side and resistivity zone greater than 150 Ω-m on the western side can be interpreted as the Cholan Formation and non-consolidated gravel, respectively. Local higher resistivity zone, near eastern slope surface, should be the response of isolated gravels collapsing from the higher lateritic terrace which is located on its eastern upslope. An unreasonable low resistivity zone shown as vertical distribution between position 13 and 21 m is probably affected by a man-made ditch along the foot of slope. The iso-resistivity color bands are nearly horizontal between position 0 and 13 m and above 227 m of elevation, which is interpreted as sand and clay of alluvial deposits. As a result the contact relation between rock and gravel is still not quite unclear, because the depth of resolution did not reach the bottom of gravel to the western central part of RIP-1, as shown in Fig. 5(a).

The RIP-2 is 240 m long with 6 m of electrode spacing across the 921 surface rupture. The result (Fig. 6) indicates that the formation can be easily divided into the top layer and the basal layer by their resistivity. The top layer, which is recognized as terrace gravel, has a resistivity of 80–1,200 Ω-m and is about 7–10 m in thickness and its thinnest part of terrace gravel is located between position 48 and 56 m coinciding with the 921 surface rupture. As for the resistivity of basal layer it is less than 60 Ω-m, which corresponds to muddy sandstone and shale of the Cholan Formation.

Furthermore, the base of the terrace gravel on the eastern side of 921 surface rupture is about 10 m higher than that of on the western side. This indicates that the 921 surface rupture is a preexisting thrust fault resulted from several thrusting events since terrace gravel was deposited. In addition, the ground surface on both side of the 921 surface rupture also exhibits an elevation difference of about 10 m, which implies that the 921 surface rupture was still active recently. The rock surface underneath terrace gravel is fairly gentle on the eastern side of the 921 surface rupture; it also indicates that no obvious vertical displacement occurred after the deposition of terrace gravel in this range. The resistivity around inferred fault plane (white dotted line in Fig. 6) is higher than that of both footwall and hanging wall, which implies the reduced porosity of rocks under compression (Cheng 2000).

Near the RIP-1 profile, 3D RIP survey with an electrode spacing of 3 m can reach greater depth than that of the RIP-1 in detecting the depth of bottom of gravel. To eliminate the effect of topography, a significant relief on the ground surface was leveled. A man-made ditch along the foot of slope was also removed to avoid contamination in resistivity of RIP-1. The salient feature is that a relatively high resistivity zone shows a westward inclination, which is interpreted as non-consolidated gravel (Fig. 7). Therefore the variation of gravel resistivity depends on water content

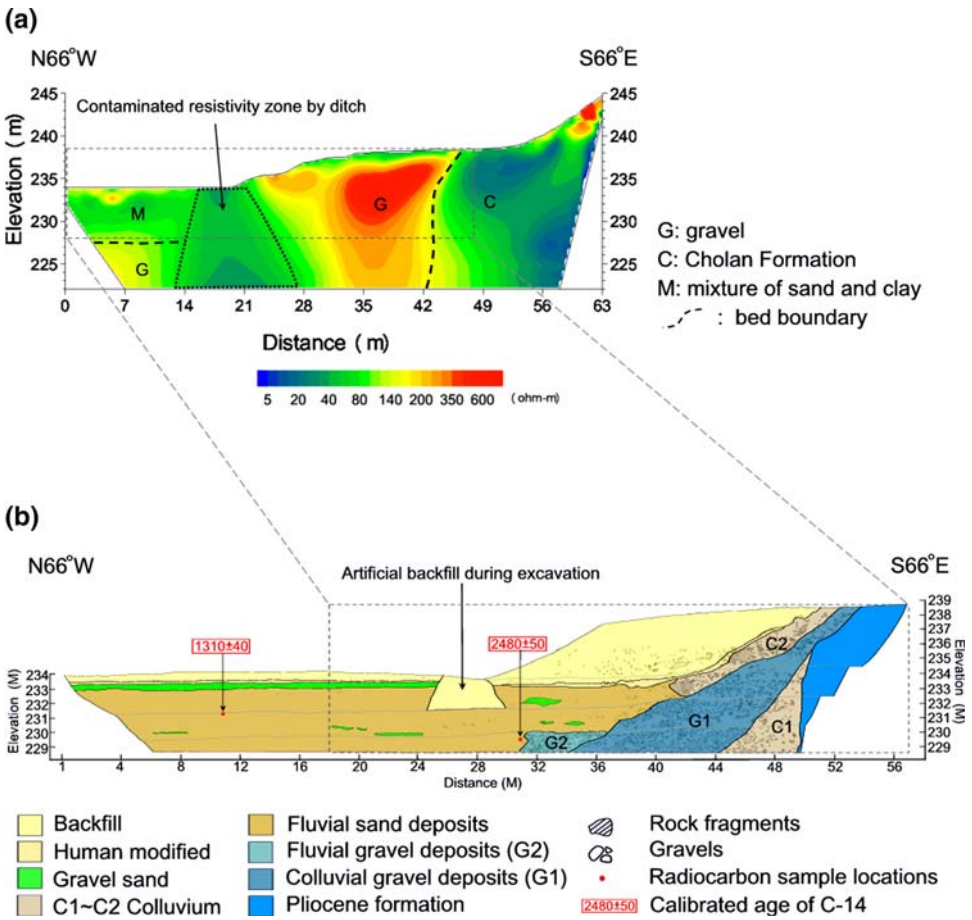

Fig. 5 Comparison between 2D RIP-1 and trench results (**a**). The interpreative result of 2D RIP-1 (**b**). Sketch of trench-wall. The approximately vertical boundary between Pliocene basement and scarp-induced colluvial deposits that show wedge-shape, while the fluvial deposits display horizontal form. No offset or disturbance was found through the trench profile

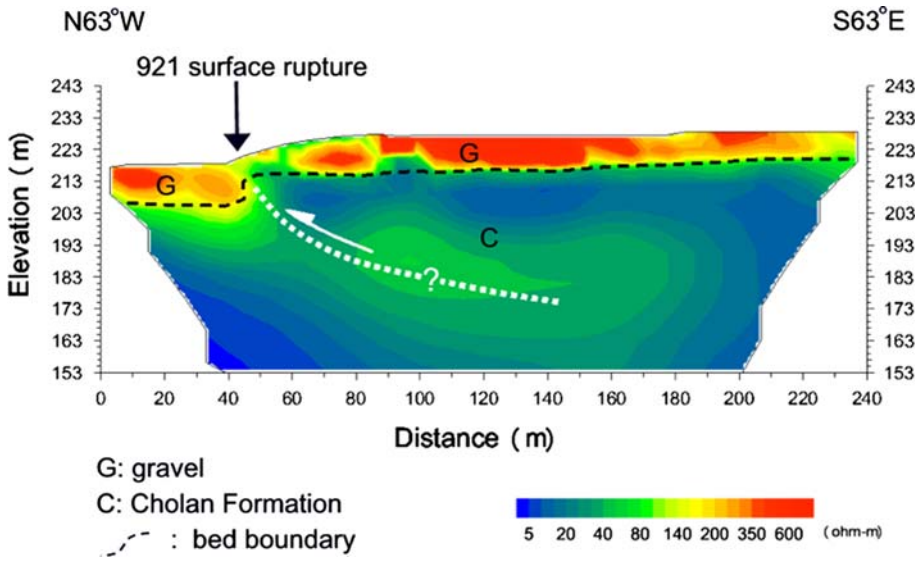

Fig. 6 The interpreative result of 2D RIP-2

and matrix content. The geometry of gravel is almost consistent in Y-Z profile along X direction (parallel to the strike of slope) and the basal depth of the gravel was estimated at 15–20 m below the surface (Fig. 7). The geometry of gravel from 3D RIP could explain the gravel deposited on the foot of slope is colluvium-induced rather than tectonic movement. The eastern border of gravel seems to have a vertical contact with the lower resistivity of the Cholan Formation within 12 m below the surface, as shown by the RIP-1. At shallower depth in the western part of 3D RIP, the horizontal iso-resistivity color bands with relatively low resistivity represent a mixture of sand and

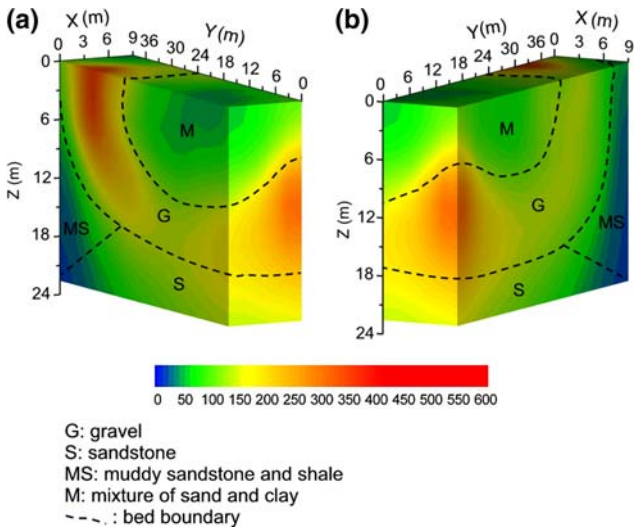

Fig. 7 The interpreative result of 3D RIP. **a** Viewed from northwest direction. **b** Viewed from southwest direction

clay, which is similar to the western part of RIP-1. Further as shown in Fig. 7, the resistivity of rock underlying the gravel between position 0 and 27 m (along X direction) is higher than that of muddy sandstone and shale in the east side of gravel, which could be correlated with relatively coarse-grained sandstone even though there is no evident resistivity boundary between them.

Trenching excavation

Trenching excavation is the best way to study recently paleoseismic fault cutting through alluvial deposits. The trench site is located on the margin of slope (Fig. 2), which was suspected of a fault scarp but had no damage during the 921 Chi-Chi Earthquake. The depth of the trench is about 6–10 m below the surface and 56 m in length. In the easternmost part of the profile (Fig. 5(b)), the Pliocene Formation consists dominantly of muddy sandstone and shale without fracture; only very thin-bedded shear gouge was found along the bedding plane with N76°E/26°SE in attitude. The wedge-shaped colluviums are composed of angular to subangular rock fragments and well-rounded gravels; the amount of rock fragments is greater than gravels, their size ranged from centimeters to tens of centimeters. The clasts of gravel bed were ranged from 1 to 20 cm in diameter and well-rounded. The differences between G1 and G2 gravel bed are listed: (1) The matrix content of G1 is clayey-silty sand, whereas G2 is medium-coarse sand; (2) the sorting of clast-supported G2 gravel bed is better than that of G1; (3) a small amount of rock fragments is visible only in G1 gravel bed. The wedge-shaped G1 gravel bed implies a scarp-induced colluvial deposit as in its eastern colluvium. The constitution and geometry of G2 gravel bed indicate that G2 was formed in a fluvial environment. Furthermore, the lower sequence of horizon overlying gravel beds is well sorted and loose; it consists of 4-m-thick brown sand with thin-bedded silt and gravel sand. This is interpreted as fluvial deposits which easily collapsed during excavation. The size and amount of sparse gravel within sand bed gradually decrease from east to west; this implies that the gravel came from the upslope during the deposition of sand bed. The upper part of the gravel sand and human modification also show a good horizontal continuity in the trenching profile. Two charcoal samples from the sand bed yield estimated ages of 1,310 ± 40 and 2,480 ± 50 year B.P. which reflect their different elevation of deposition (Fig. 5(b)).

The feature of the scarp formed by the Pliocene Formation in the trenching profile is similar to the 2D and 3D RIP profiles showing a steep contact relation between rock of lower resistivity and gravel/colluviums of higher resistivity in shallow subsurface. Throughout the profile, the layers above the rock have no offset and disturbance by fault. However, due to the limited depth of excavation, no evidence of rock structural relation at depth can be observed. Hence, whether the rock scarp is fault-generated is still uncertain.

Borehole sampling

Four continuously cored boreholes, BH-1–BH-4 (Fig. 2), were selected and drilled to the depth of 30–80 m. To avoid the limitation of rice field during irrigation, the locations of boreholes were shifted to the south of trench site. The aims of boreholes are to find out the thickness of gravel, depth of rock surface, lithological variations of rock, and degree of disturbance by suspected faults.

The elevation of boreholes BH-2, BH-3, and BH-4 were treated as the same. The borehole profile (Fig. 8) shows that the elevation of rock surface obtained from boreholes, except for BH-1, gradually decrease eastward to the foot of slope where the rock surface is highly varied. It seems that the variation of thickness of gravel is the same as rock surface. The result of borehole BH-4 indicates that the rock surface of the foot of slope is 16.8 m below the surface which is quite consistent with estimation from 3D RIP. However, the difference of 17.5 m in the rock surface, with the short distance between boreholes BH-1 and BH-4, also displays the steep rock surface below the slope. Interpretation of 2D and 3D RIP clearly demonstrates this feature.

Based on the lithologic characteristics, the rock can be divided into two layers: (1) the dominantly muddy sandstone and shale with weak to intense bioturbations; (2) light-grey, massive and fine- to coarse-grained sandstone mixed

with some thinly layered shale, bioturbations with abundant trace fossils, and transported shell fragments are also distributed. The former is the predominant rock in this site; the latter can be served as a marker to analyze the geological structure between boreholes. Based on the correlation of cores, the sandstone (over 20 m in salient thickness) contains transported shell fragments both in boreholes BH-1 and BH-4. Moreover, the rock in the upper part of the BH-1 also shows consistent bedding dip and few fractures in it. This indicates that these strata beneath the toe of the slope were not disturbed or offset by faults.

By contrast, boreholes BH-2, BH-3, and the lower part of the BH-1, frequently show fractured and sheared features which are similar to fault-related rock (Huang et al. 2002; Tanaka et al. 2002; Song et al. 2007), such as shear gouge with sub-millimeters to centimeters in thickness and few to highly dense fracture filled with shear gouge. The dip angle in the rock of boreholes BH-2 and BH-3 is around 30–40 degrees which is steeper than that of boreholes BH-1 and BH-4. The irregular bedding dip also can be seen in part of rock samples. It indicates that this part of stratum must be highly related to intensely tectonic movement, very possibly to form faults before the deposition of gravel.

Discussion

The resolution of RIP methods, as prior expectation, is enough to detect the geometry of gravel and surface between gravel and rock, which was also verified by geological data. However, the contrast in resistivity between sheared rock and its host rock is too low to subdivide. So, the resistivity data is not enough for identifying the definite location of shear zone. Further due to the resistivity is contaminated by the N–S trending high-tension power line between RIP-1 and RIP-2, the detailed geometry of gravel and rock surface is thus obscure. Nevertheless, all the productive groundwater wells owned by local farmers are located between the toe of slope and borehole BH-2 where aquifer formed by filluvial deposits near N–S trending paleochannal. Therefore, the thicker filluvial deposits and deeper rock surface can be expected.

The wedge-shaped gravel and colluviums, and horizontal sand bed in trenching profile demonstrated that the paleostream had already developed along the toe of slope. However, both results of boreholes and trenching excavation beneath the toe of the slope indicated that rock and overlying soil deposits were not disturbed by fault. In addition, the surface of lateritic terrace located on top of slope also exhibits a westward tilt implying that it was not affected by fault, at least recently. Thus, the incision of paleostream should be responsible for the steep and deep rock surface beneath the slope and the toe of slope.

The geological profile is striking N76°E, which is similar to bedding plane measured in the trenching profile. So, the sandstone with transported shell fragments obtained from boreholes BH-1 and BH-4 should supposed be displaying a subhorizontal apparent dip and extended to the upper part of BH-2, which is obviously not so, as shown in Fig. 8. It is assumed that this sandstone and overlying rock between the boreholes BH-1 and BH-2 may be uplifted by reverse faults that extend to the location of boreholes BH-2 and BH-3. If it is the case, the paleostream was developed along the foot of

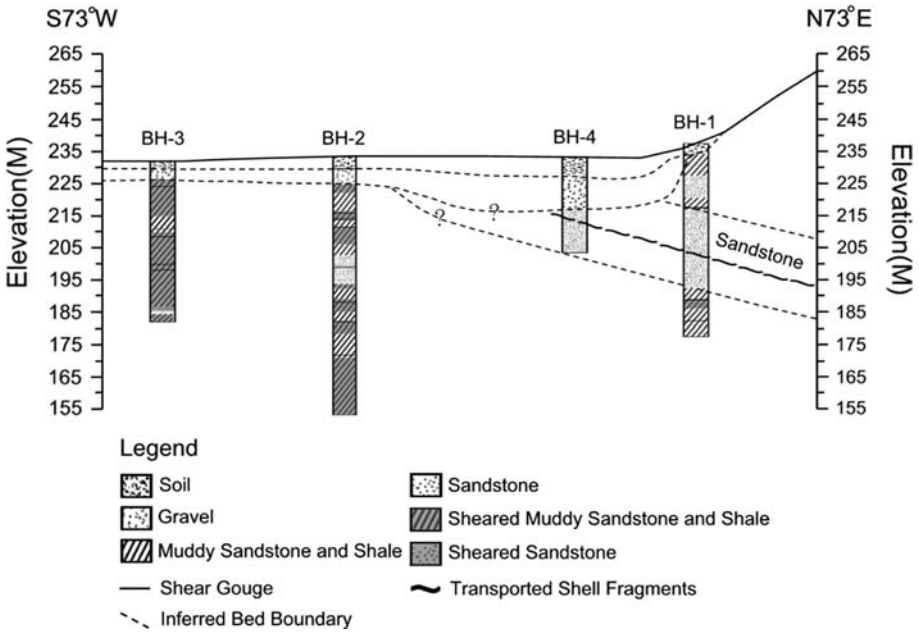

Fig. 8 The profile of borehole data. The shadowed area represents the fractured and sheared rocks, which appear more frequently in boreholes BH-2 and BH-3 than BH-1 and BH-4

fault scarp, which was subjected to erosion and led to the subsequent retrogression or retreat of the slope. Thus, it is obvious that the active reverse fault already shifted westward to 921 surface rupture, and every shallowed reverse fault in this range should belong to the imbricate splay fault system, as suggested by Huang et al. (2000). The rock shown in TCU102 borehole (Sino Geotechnology Incorporation (Sino Geotech) 2002) (Fig. 1), located on about 600 m to the west side of 921 surface rupture, is GL-14 m (about 210 m elevation), and it signified that the Chelungpu fault is situated to the west of this borehole.

The degree of sheared rock sample of BH-2 and BH-3 is stronger than that of BH-1 and BH-4. Therefore, the fault around areas of boreholes BH-2 and BH-3 can be expected, and it may suggest that high amount of offset and many fault events were formed before the deposition of gravel, even though no topographic features appear at present.

The ridge formed by hogback and cuesta landforms clearly displays the changed direction from N–S trending (southwest of Wuniulan River) to NE–SW trending (northeast of Wuniulan River), as well as the attitude of bedding plane on the both sides of Wuniulan river, especially near the 921 surface rupture (Fig. 1). It may be related to N30–40°W slip direction of 921 surface rupture in this area (Chen et al. 2000, 2001, 2003). It indicates that the variation in strike of bedding plane is a very important factor for the turning of 921 surface rupture in the study area.

Furthermore, since the vertical displacement along the 1999 surface rupture is 3–4 m in the study area, the elevation differences of 10 m of the basal gravel obtained from RIP-1 may suggest the occurrence of two prior events at least on the present trace.

Finally, the elevations of two charcoal samples from the sand bed of the trench are 231 3 and 229.5 m, respectively. The sand bed is higher than the top of gravel in elevation, and should be visible above the gravel of the non-lateritic terrace. The age of the sand bed demonstrates that the strata were not affected by fault, at least since 2,480 ± 50 year B.P. On the other hand, the fine-grained fillings in fault-related rocks is quite consolidated; this also implies that the fault was formed very long time ago.

Conclusion

Based on RIP and geological data, the following conclusions can be drawn:

1. From east to west, the rock surface of the study area shows steep, deeper, gentle and subvertical displacement beneath the slope, the toe of slope, the non-lateritic terrace, and 921 surface rupture, respectively.
2. The fault-related rock found in the boreholes BH-2 and BH-3 is located on a flatly non-lateritic terrace where the rock surface is fairly gentle, and the faults occurred before deposition of terrace gravel.
3. The slope with N20°E trending topographic feature, east of the 921 surface rupture, was not directly caused by fault. However, it was formed in both the process of retrogressive or retreat of the fault scarp and the incision of paleostream generating concave-shape rock surface beneath the toe of the slope. The younger age of the horizontal sand bed in the trenching profile was also not affected by fault that formed around boreholes BH-2 and BH-3.
4. 921 surface rupture occurred on a preexisting fault where the quality of resistivity data is good for interpretation. It may suggest the occurrence of at least two prior events on the present trace. However, the 921 surface rupture formed by Chi-Chi earthquake is an unquestionable and highly active fault. So, it is not necessary to establish an extra restricted zone for buildings in the study area, except the 921 surface rupture.

Acknowledgments We are grateful to Sino Geotechnology (Sino Geotech) lnc for generously provided geological data for this study. We also thank the engineers at Sino Geotech for help with the fieldwork.

References

Bonilla MG (1977) Summary of quaternary faulting and elevation changes in Taiwan. Mem Geol Soc China 2:43–56

CGS (Central Geological Survey) 1999 Report of the geological survey of the 1999 Chi-Chi earthquake. Cent Geol Surv, Taipei, Taiwan. 315 pp (in Chinese)

Chang SL (1971) Subsurface geologic study of the Taichung basin, Taiwan. Petrol Geol Taiwan 8:21–45

Chang HC, Lin CW, Chen MM, Lu ST (1998) An introduction to the active faults of Taiwan. Spec. Publ. Cent. Geol. Surv, Taipei, Taiwan. 10: 103 pp

Chen WS, Chen YG, Liu TK, Huang NW, Lin CC, Sung SH, Lee KJ (2000) Characteristics of the Chi-Chi earthquake ruptures. Spec Publ Cent Geol Surv Taipei Taiwan 12:137–154

Chen WS, Huang BS, Chen YG, Lee YH, Yang CN, Lo CH, Chang HC, Sung QC, Huang NW, Lin CC, Sung SH, Lee KJ (2001) 1999 Chi-Chi earthquake: a case study on the role of thrust-ramp structures for generating earthquakes. Bull Seismological Soc Am 91:986–994

Chen WS, Chen YG, Shih RC, Liu TK, Huang NW, Lin CC, Sung SH, Lee KJ (2003) Thrust-related river terrace development in relation to the 1999 Chi-Chi earthquake rupture, Western Foothills, central Taiwan. J Asian Earth Sci 21:473–480

Cheng PH (2000) Imaging the subsurface structure of northern tip of the 1999 Chi-Chi earthquake fault in central Taiwan using electrical resistivity method. Terr Atmos Ocean Sci 11:721–734

Cheng PH, Yang CH, You JI, Shieh JS (2002) An electrical resistivity study of the Chelungpu fault in the Tasotun area, central Taiwan. Terr Atmos Ocean Sci 13:375–386

Ho CS (1959) Thrust structure in Taichung and Nantou, central Taiwan. Bull Geol Surv Taipei Taiwan 11:65–80

Ho CS (1976) Foothill tectonics of Taiwan. Bull Geol Surv Taipei Taiwan 25:9–28

Ho HC, Chen MM (2000) Explanatory text of the geological map of Taiwan, sheet 24: Taichung. Centr. Geol. Surv, Taipei, Taiwan. ROC

Hsu TL, Chang HC (1979) Quaternary faulting in Taiwan. Memoir Geol Soc China 3:155–165

Huang ST, Wu JC, Hung JH, Tanaka H (2002) Studies of sedimentary facies, stratigraphy, and deformation structures of the Chelungpu fault zone on cores from drilled wells in Fengyuan and Nantou, central Taiwan. Terr Atmos Ocean Sci 13:253–278

Huang WJ, Chen ZY, Liu SY, Lin YH, Lin CW, Chang HC (2000) Surface deformation models of the 1999 Chi-Chi earthquake between Tachiachi and Toupienkengchi, central Taiwan. Spec Publ Cent Geol Surv Taipei Taiwan 12:63–87

Lai KY, Chen YG, Hung JH, John S, Yue LF, Chen YW (2006) Surface deformation related to kink-folding above an active fault: evidence from geomorphic features and co-seismic slips. Quat Int 147:44–54

Lee JF (2000) Explanatory text of the geological map of Taiwan, sheet 18: Tungshih. **Centr Geol Surv, Taipei, Taiwan

Loke MH, Barker RD (1996) Rapid least-squares inversion of apparent resistivity pseudosections by a quasi-Newton method. Geophys Prospect 44:499–524

Loke MH (2001) Tutorial: 2D and 3D electrical imaging surveys. Penang, Malaysia, Universiti Sains Malaysia, Unpublished course notes, http://www.geoelectric.com

Meng CY (1963) San-I overthrust. Petrol Geol Taiwan 2:1–20

Nguyen F, Garambois S, Chardon D, Hermitte D, Bellier O, Jongmans D (2007) Subsurface electrical imaging of anisotropic formations affected by a slow active reverse fault, Provence, France. J Appl Geophys 62:338–353

Ota Y, Watanabe M, Suzuki Y, Sawa H (2003) Active faults along the Chelungpu fault, central Taiwan, especially its close coincidence in the location of 1999 Chi-Chi earthquake fault. J Geogr 112:18–34 (in Japanese)

Ota Y, Watanabe M, Suzuki Y, Sawa H (2004) Geomorphological identification of pre-existing active Chelungpu fault in central Taiwan, especially its relation to the location of the surface rupture by the 1999 Chi-Chi earthquake. Quat Int 116:155–166

Ota Y, Shishikura M, Ichikawa K, Watanabe M, Yanagida M, Tanaka T, Sawa H, Yamaguchi M, Lee YH, Lu ST, Shih TS, Amagasa S (2007) Low-angle reverse faulting during two earthquakes on the northern part of the Chelungpu fault, deduced from the Fengyuan trench, central Taiwan. Terr Atmos Ocean Sci 18:55–66

Pan YS (1967) Interpretation and seismic coordination of the Bouguer gravity anomalies over west-central Taiwan Petrol. Geol Taipei Taiwan 5:99–115

Sino Geotechnology Incorporation (Sino Geotech) 2002 Geological survey of strong motion stations (in Chinese). Report to National Centre for Research on Earthquake Engineering (NCREE), Taipei, Taiwan

Song SR, Kuo LW, Yeh EC, Wang CY, Hung JH, Ma KF (2007) Characteristics of the lithology, fault-related rocks and fault zone structures in TCDP Hole-A. Terr Atmos Ocean Sci 18:243–269

Suzuki K, Toda S, Kusunoki K, Fujimitsu Y, Mogi T, Jomori A (2000) Case studies of electrical and electromagnetic methods applied to mapping active faults beneath the thick quaternary. Eng Geol 56:29–45

Tanaka H, Wang CY, Chen WM, Arito S, Kotaro U, Ito H, Masataka A (2002) Initial science report of shallow drilling penetrating into the Chelungpu fault zone, Taiwan. Terr Atmos Ocean Sci 13:227–251

Tsai H, Sung QC (2003) Geomorphic evidence for an active pop-up zone associated with the Chelungpu fault in central Taiwan. Geomorphology 56:31–47

Vanneste K, Verbeeck K, Petermans T (2008) Pseudo-3D imaging of a low-slip-rate, active normal fault using shallow geophysical methods: the Geleen fault in the Belgian Maas River valley. Geophysics 73:B1–B9

Yang CH, Cheng PH, You JI, Tsai LL (2002) Significant resistivity changes in the fault zone associated with the 1999 Chi-Chi earthquake west-central Taiwan. Tectonophysics 350:299–313